Electroosmotic flow in nanoporous membranes in the region of electric double layer overlap

*Hannah Leese and Davide Mattia**

Department of Chemical Engineering, University of Bath, Claverton Down, Bath, BA1 7AY, United Kingdom.

Corresponding Author: E-mail: D.Mattia@bath.ac.uk,

Fax: +44(0)1225385731; Tel:+44(0)1225383961

Abstract

This study investigates electroosmotic (EO) flow with sodium tetraborate buffer in nanoporous anodized alumina membranes (AAMs). Membranes with pore diameters ranging from 8 to 100 nm have been fabricated with narrow pore size distributions to systematically investigate the effect of pore diameter on the EO pumping down to the electric double layer overlap region. EO flow was observed in membranes with pore diameters in and below this region, along with evidence of concentration polarization (CP), which resulted in a significant reduction in flux. The initial flux, though, could be fully recovered by temporarily reversing the flow and dislodging the accumulated ion layer from the feed side of the membrane. Stable pumping for up to 2 hours was obtained before any flux reduction caused by CP was observed.

Keywords Electroosmosis, electric double layer, electroosmotic mobility, concentration polarisation, borate buffer.

1. Introduction

Electroosmosis, the bulk movement of an electrolyte in a charged channel under an externally applied electric field, is widely used as a pulse-free, no-moving parts pumping method for lab-on-a-chip and microfluidic applications (Chuan-Hua and Santiago 2002; Takamura et al. 2003; Prakash et al. 2006). To increase the total flow-rate and pressure capabilities of EO pumps a parallel channel configuration can be used (Bruus 2007), in other words a membrane. A number of publications on electroosmotic flow (EOF) in inorganic membranes have concentrated on the effects of the membrane surface structure and charge, the results of which have been summarised in Table 1. High flow/high pressure EO pumps were made using silica and alumina frits, with average pore diameters ranging from 50 nm to 2 μm and a phosphate buffer of pH 10.3 with 2 mM NaCl (Prakash et al. 2006). The flow to pressure ratio decreased exponentially with pore diameter for both materials, though little effect on pressure and flow was observed with ionic strength. Similar results have been obtained for EOF rates of borate buffer through glass frit discs (Yao et al. 2003) and so-called microchannel glass plates (Cao et al. 2012). A much higher flow rate per unit applied voltage and unit area was observed for a borate buffer flowing through silicon membranes with ~3 μm pores (Yao et al. 2006). Coating of the silicon pores with silica significantly decreased the maximum flow rate achieved. The materials used in all these studies are characterized by a large pore size distribution, as noted elsewhere (Yao et al. 2003).

EO measurements using KCl as an electrolyte and commercial asymmetric anodized alumina membranes (AAMs) sold as Whatman ® Anodisc^{TM} looked at the effect of pore diameter (200 nm on one end and 20, 100 and 200 nm at the other end) on flow rate, with slight increases with decreasing pore size (Chen et al. 2008a). The study observed an increase in flow rate for all pore diameters with increasing applied voltages. Interestingly, they observed a decrease in flow rate with increasing concentration of electrolyte, which is contrary to other EO studies, as concentration polarisation (CP) effects would be expected in systems with such low electrolyte concentration. These commercial membranes, normally used as filters for aggressive organic media, have a significant amount of branching as well as large pore size distributions, further complicating the evaluation of experimental results. EO measurements for de-ionized water in the same commercial AAMs, but with constant 200 (± 50) nm average pore diameter throughout the membrane thickness (and with significant branching), showed higher flow rates per unit voltage and unit area than the previous publication (Chen et al.

2010). The authors also found that the flow rate decreased with decreasing porosity, as expected. The effect of surface charge on EOF was observed with a two-orders-of-magnitude increase in the maximum flow rate for SiO_2-coated AAMs compared to uncoated AAMs using a borate buffer (Vajandar et al. 2007). Another study looked at the effect of three different AAM pore diameters of 25, 46 and 240 nm) on ion transport and found that ion diffusion coefficients decreased with decreasing pore diameter for ions with the same charge as the pore wall (Romero et al. 2012).

All of the above results are for membranes with relatively large pore diameters. This is key, as classical electro-kinetic models require that the pore radius ($D_P/2$) be larger than the electric double layer (EDL) thickness (also known as the Debye length, λ_D) for any electroosmotic flow to be observed. The Debye length is defined as the thickness of the polarized layer of ions adjacent to a stationary charged surface (Chang and Yeo 2010), and can be calculated (for a monovalent binary electrolyte) by the Debye-Hückel approximation, Eq. 1:

$$\lambda_D = \sqrt{\frac{\varepsilon k_b T}{2(ze)^2 c_0}} \tag{1}$$

where k_b, and T are the Boltzmann constant and temperature, respectively; c_o, e and z are the concentration, electronic charge and valence of the ions, respectively; $\varepsilon = \varepsilon_r \varepsilon_0$, where ε_r and ε_0 are the relative permittivity of the electrolyte and the vacuum permittivity, respectively.

Table 1 Literature Values for EOF in silica, glass and alumina membranes

Q_{EO} (10^{-3} $m^3s^{-1}V^{-1}m^{-2}$)	Material	Pore diameter, D_P (nm)	$2\lambda_D/D_P$	Electrolyte Conc. (10^{-3}M)	ref.
1.3	Silicon	2000	~0.01	$Na_2B_4O_7$, 1.0	Yao et al. 2006
0.5	sintered glass	550	~0.04	$Na_2B_4O_7$, 1.0	Yao et al. 2003
0.0125	silica	600	~0.03	NaCl, 2.0	Prakash et al. 2006
0.02	SiO_2-coated AAM	70	~0.17	$Na_2B_4O_7$, 2.5	Vajandar et al. 2007
0.003	AAM	80	~0.15		
0.0015	Anodisc™	200/100	~0.30	KCl, 10^{-4}	Chen et al. 2008
0.016	Anodisc™	200	~9.60	DI Water	Chen et al. 2010

Several theoretical studies have looked at the effect of EDL overlap, $D_P \leq 2\lambda_D$, on EOF predicting that as EDLs approach each other and overlap, the entire channel becomes charged and the expected 'plug-like' velocity profile reduces back to a parabolic one (Bruus 2007; Huang and Yang 2007; Rice and

Whitehead 1965). Simulations of EOF in 6.5 nm diameter channels showed that ions in the stern layer were not fixed to the channel walls and that the viscosity increased by a factor of 6 in the first nanometre closest to the wall (Freund 2002). Simulations of EO in nanotubes with high surface charge densities found that with increase in surface charge density, both the thickness of the EDL and the peak height of the counter-ion density increased (Chen et al. 2008b); this was also confirmed directly by AFM measurements (Besteman et al. 2004). However, a recent experimental study has produced a carbon nanotube (CNT) membrane with diameters ranging from 1.5 to 7 nm and found that when CNTs were functionalized, highly efficient flow rates compared to other EO pumps could be obtained (Wu et al. 2011). It is likely that the EDLs were overlapped in this study as the concentrations of buffer would produce Debye lengths of ~ 5-10 nm. Measurements in track-etched polymer membranes with pores of approximately 15 nm showed the persistence of EOF close to, but not beyond, the electric double layer overlap region (Kemery et al. 1998). An experimental estimation of the magnitude of electroosmotic flow in the EDL overlap region is further complicated by practical limitations and by the presence of physical effects which prevent stable EOFs such as electrolysis and concentration polarisation (CP) (Erlandsson and Robinson 2011; Strickland et al. 2010). While the Debye length can be significantly increased by reducing the concentration of the electrolyte (thereby allowing observation of EO and EDL of larger pore diameters), this induces significant amounts of electrolysis and gas evolution (Brask et al. 2005). In addition, CP is expected to be significant in nanoscale channels, severely shortening the lifetime of the EO pump (Strickland et al. 2010; Suss et al. 2011).

In this publication, experimental results on EO pumping using bespoke AAMs with tortuosity approaching unity are presented. Membranes with pore diameters ranging from 8 to 100 nm have been fabricated with narrow pore distributions to systematically investigate the effect of pore diameter on the EO pumping down to the EDL overlap region. EOF was clearly observed in membranes with pore diameters in and below this region, along with significant concentration polarization effects. The CP effects, though, were found to be reversible, with a complete regeneration of the original EO flow and stable pumping for up to 2 hours.

2. Experimental Methods

2.1 Membrane Fabrication

The AAMs were prepared by a well-established two-step anodization method (Masuda and Fukuda 1995). Aluminium discs with 13 mm diameter (99.99%, 0.1 mm or 0.25 mm thickness, Alfa Aesar) were annealed in air at 500 °C for 1 hour (CWF1100, Carbolite). The annealed discs were degreased by ultra-sonication in HPLC grade acetone (>99.5%, Fisher) and electropolished in a 1:4 volumetric ratio of perchloric acid (60-62%, Fisher) and ethanol (96%, Fisher). The solution was kept below -50 °C by a dry ice/acetone bath and 20 V was applied for 15 minutes. The now shiny aluminium discs were anodized in 0.5 and 1.0 M sulfuric acid or 0.3 M oxalic acid. The concentration and type of acid used depended on the applied anodization voltage. The potentiostatic anodization voltage applied ranged from 10 to 80 V. The temperature was controlled to ± 0.1 °C accuracy between 0 and 14 °C, this value also depended on anodization voltage and electrolyte type. The first-step anodization was performed for 30 minutes to 1hour; the formed oxide layer was then removed by wet chemical etching using a 1:1 mixture of 6wt% phosphoric acid and 1.8wt% chromic acid at 60 °C for an equivalent time to the first-step. The aluminium was washed thoroughly in deionized water and placed back into the same anodization conditions as previously described but for a period of 5 to 6 hours for sulfuric acid and 10 to 12 hours for oxalic acid. The remaining aluminium which had not been anodized was removed by a 1:1 volumetric solution of 0.2 M copper (II) chloride and 20% hydrochloric acid. This exposed the barrier layer of the alumina, which was etched away using 6wt% phosphoric acid by an electrochemical detection method adapted from (Lillo and Losic 2009; Lee et al. 2012).

In addition to the two-step fabrication method of AAMs, a ramping anodization method was utilised to produce pore diameters < 10 nm. This was to overcome the severely reduced robustness of the AAMs with smallest diameters (i.e. when the potentiostatic voltage was 5 to 8 V). AAMs with pore diameters < 10 nm were desirable to probe the effect of EDL overlap. To do this an initial voltage of 24 V was applied for a period of 4 hours, this was then ramped down to 5 V at a rate of 0.4 V min^{-1} and anodized for a further 2 hours. This method was adopted from (Lee and Mattia 2013). This asymmetric membrane was the only way to obtain AAMs mechanically robust enough to withstand the EOF experiments and probe EDL overlap. The side of the AAM with smallest pore diameter faced the feed side of the EOF, therefore controlling the flow rate.

2.2 Membrane Characterisation

At least three AAMs were prepared for each anodization voltage and six for the AAMs produced via ramping. The surface morphology and cross-section of the AAMs was characterized using a JEOL FESEM6301F field emission scanning electron microscope (FESEM). The samples were not coated for SEM imaging. Statistical image analysis of SEM micrographs using ImageJ software was used to characterize average pore diameter, porosity and pore size distribution. An in-depth discussion of the statistical analysis of AAMs can be found in (Lee et al. 2012). AFM was utilised to image the smallest pore diameters, these were analysed using Gwyddion Software. All membranes were analysed post-EOF experiments; therefore degradation of the material would have been obvious. AAMs which snapped during the process were disregarded as the mechanical integrity of the membrane structure had failed. Details of the AAMs pore diameter, thickness and porosity can be found in the supplementary information.

2.3 Membrane Holder and EO experiments Design

The electroosmotic flow measurements through the AAMs were conducted using a custom-made rig and membrane holder. The membrane holder was made of two polycarbonate and acrylic flanges with 60 ml chambers on either side which held the buffer solution (Fig. 1). The AAM was placed between the two vessels with an 8 mm effective diameter. To ensure good sealing the membrane was clamped between silicone rubber annuluses. Platinum mesh (99.99%, 52 mesh per inch) was used for the electrodes and clamped either side of the AAM sealed by more silicone annuluses to ensure no electrical connection was possible between the meshes but only through the membrane pores. The holder was then connected to the custom-made rig for the electroosmotic flow measurements. Pressure transducers (Swagelok industrial standard®, 0.05 Bar error) were placed before and after the membrane holder (and chambers) to measure the pressure drop across the membrane. Small pressure gradients were exerted across the AAMs (18 – 50 kPa) to record pressure-driven flow before the application of the electric field to probe the structural integrity of the membrane. The pressure gradient was then maintained constant throughout the EOF measurement to act as a reference. A reservoir was placed at the feed side of the membrane which could be pressurized when a higher pressure was necessary for the flow measurements. A thermocouple was also inserted in the rig to monitor the temperature of the liquid so changes in viscosity could be accounted for. A high precision mass balance (Fisherbrand, FB73650, 0.1 mg sensitivity) recorded the droplet rate, whereby the flow rate was

calculated. A layer of oil was added to the collection beaker to prevent evaporation. Sodium tetra-borate, $Na_2B_4O_7$, pH 9.2, was used as the buffer during the experiments. The concentration of the aqueous electrolyte was varied from 2 to 10 mM and the applied voltage for the electroosmotic measurements ranged from 10 to 40 V using a power supply (Agilent technologies, 6645A) and was recorded by a computer using automated data acquisition equipment (Semaphore Systems, ADAM-4017) and Lab View software. Each measurement was repeated at least three times. The experiments were run for at least 20 minutes, and up to 2 hours. In most cases after 20 to 40 minutes, the electroosmotic pumping rate would decrease to laminar flow or less. It is believed this is due to concentration polarisation and buffer depletion, and will be discussed later in further detail.

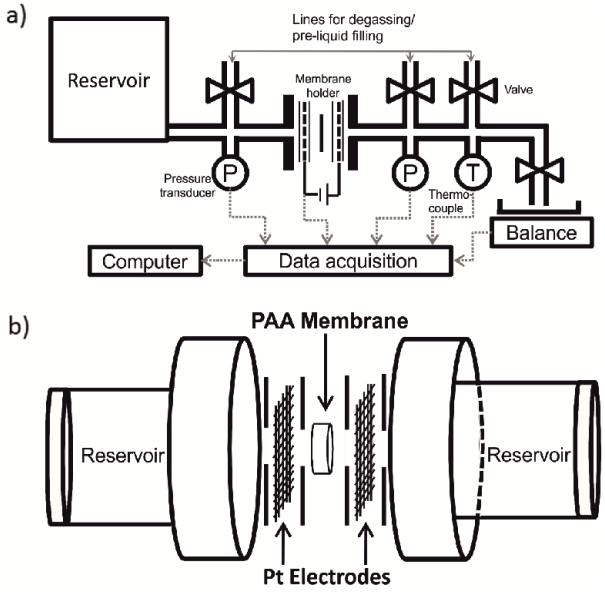

Fig 1. Schematic of the custom-made a) electroosmotic rig and b) membrane holder.

2.4 Analysis of Results

As discussed, a small pressure-driven flow was superimposed to the EOF to quantitatively evaluate the EO and concentration polarization effects. Therefore, the flow rate through a porous membrane with cylindrical pores under an applied electric field and pressure gradient, exerted in the same direction, can be expressed as (Vajandar et al. 2007; Zeng et al. 2001; Rice and Whitehead 1965):

$$Q_T = \frac{\phi}{\tau} A \left(\frac{D_p^2}{32\eta L} \Delta P + \frac{\varepsilon \zeta}{\eta} \frac{\Delta V_{eff}}{L} \right) \equiv Q_{\Delta P} + Q_{EO} \qquad (2)$$

where ϕ is the porosity of the porous membrane, τ the tortuosity of the membrane pores and A the

effective membrane area. ΔP is the applied pressure difference across the membrane, D_P the pore diameter and L the thickness of the membrane; η the viscosity; ζ is the zeta potential, and ΔV_{eff} is the effective voltage drop across the membrane. The electroosmotic mobility is defined as:

$$\mu_{EO} = \frac{\varepsilon\zeta}{\eta} \equiv \frac{u_{EO}}{E} \tag{3}$$

where $u_{EO} = Q_{EO} / (\phi A)$ is the electroosmotic pore velocity (the velocity in a single membrane pore) and $E = \Delta V_{eff} / L$ is the effective electric field.

The zeta potential, ζ, was calculated from streaming potential measurements, using the Helmholtz-Smoluchowski equation from experimental data (see Eq. S1 in the supplementary information). The streaming potential measurements were carried out in the electroosmotic rig in Fig.1. The effective voltage can be calculated via the following equation:

$$\Delta V_{eff} = (\Delta V_{app} - \Delta V_{dec}) - 2R_d I \tag{4}$$

where ΔV_{dec} is the decomposition potential which is the voltage required to initiate dissociation and association electrode reactions, and was found to be ~ 4.5 V for a platinum electrode/borate buffer system (Yao et al. 2003). ΔV_{app} is the applied voltage, R_d the resistance between the surface of the membrane and the electrode and I the current of the system (see Fig. S3 in the supplementary information).

It is noted here that the back pressure experienced in electroosmotic flows in this study was less that 0.01% of the total flow and therefore negligible (Bruus 2007; Rice and Whitehead 1965).

3. Results and Discussion

3.1 AAM characterisation

A regular pore structure was observed for all AMMs tested, with narrow pore size distributions (Fig. 2) and tortuosity τ ~1, consistent with previous findings (Lee et al. 2012). The distribution gets narrower the smaller the pore size (Fig. S1). Similarly, the dependence of average pore diameter on anodization voltage (Sulka 2008) and the independence of the porosity with anodization voltage (Nielsch et al. 2002), are also consistent with previous findings (see Table S1 for all pore diameter, porosity, and thickness measurements of AMMs tested, Fig. S1 for pore size distributions and Fig. S2 for anodization voltage dependence). An example of the asymmetric AAMs produced via ramping the

anodization voltage down to 5 V is shown in the SEM image in Fig. 2a and has an average pore diameter of ~8 nm on the feed side. Therefore, with a borate buffer concentration of 5 mM producing a Debye length ~ 4.5 nm within the AAM channel, EO in the EDL overlap region can be analysed.

Metal oxides like alumina are amphoteric materials (they are able to gain or lose protons) and therefore the surface charge changes when exposed to acidic or basic conditions (Hunter 1981). The isoelectric point of alumina has been reported between pH 8.0 (Chen et al. 2008a; Tang et al. 2004) and pH 9.1 (Hunter 1981). In this study, therefore, alumina was negatively charged in the more basic solution of the borate buffer (pH 9.2). Counter ions (i.e. the Na^+) of the borate buffer were attracted to the channel wall of the alumina, therefore building up the EDL. When an electrical potential was applied across the membrane the excess (diffuse) counter-ions in the EDL moved towards the counter-electrode, dragging the bulk liquid, resulting in a net (plug-like) flow (Bruus 2007).

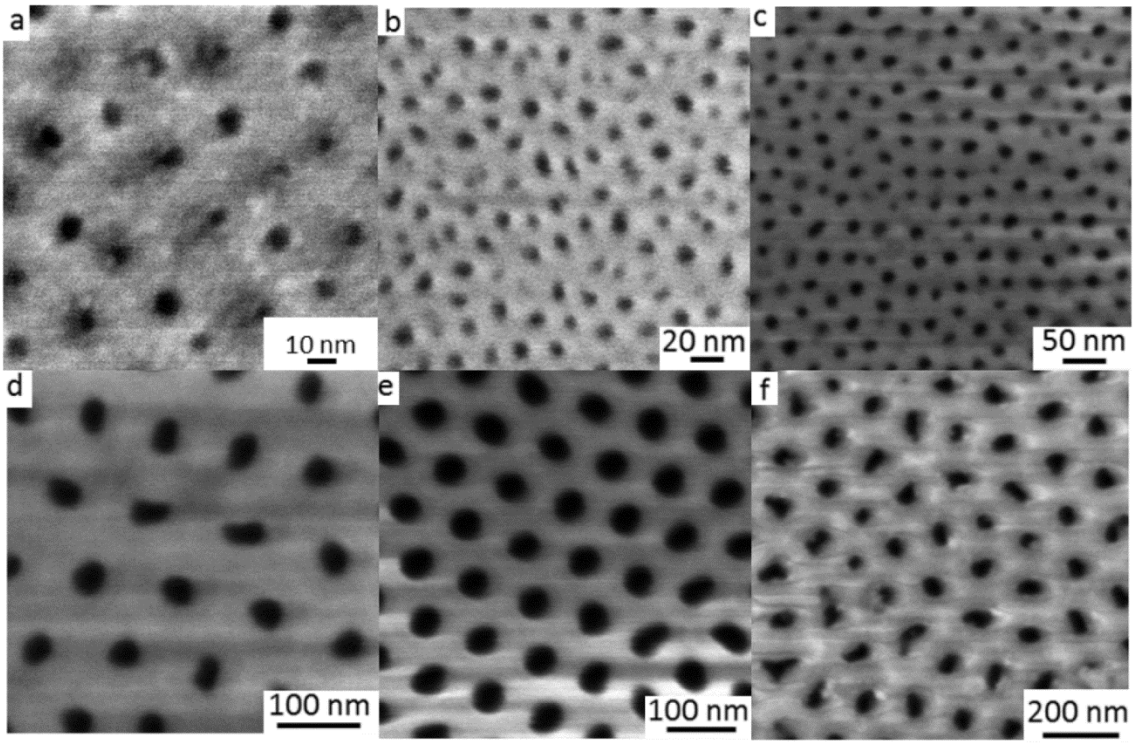

Fig 2. FESEM of AAMs under different anodization conditions of a) 0.5 M H_2SO_4, V_I = 24 V, V_F = 5 V, ~ 8 nm b) 1.0 M H_2SO_4, 10 V, D_P ~ 13 nm; c) 0.5 M H_2SO_4, 20 V, D_P ~ 24nm; d) 0.3 M $C_2H_2O_4$, 30 V, D_P ~ 36 nm; e) 0.3 M $C_2H_2O_4$, 40 V, D_P ~ 52 nm; f) 0.3 M $C_2H_2O_4$, 50 V, D_P ~ 67 nm.

3.2 Electroosmotic Flow Rates and Pore Diameter

Permeability measurements for all tested membranes under an external pressure gradient follow the Hagen-Poiseuille equation (see inset of Fig. 3), confirming the structural integrity of the membranes, in

agreement with analysis of SEM micrographs. When an electric field was applied perpendicular to the membrane, EOF was superimposed onto the pressure-driven flow (Eq. 2), resulting in an overall higher total flow rate for each pore diameter value. To account for differences in membrane thickness and applied pressure, the data is presented in terms of hydraulic permeability, $K = QL / \Delta PA$ (Fig. 3). The contribution of EOF relative to the total flow rate became more significant for smaller pore diameters, which will be discussed in further detail later. The measurements in Fig. 3 present all the points of the tested membranes, with the same applied voltage (10 V), concentration of electrolyte (5 mM sodium tetraborate) and for the same time (30 minutes). For the majority of cases, after approximately 40 minutes there was clear evidence of severe reductions in EO flow rates. The cumulative error was 5% for the flow measurements for each data point (y-axis); contributions to this include applied voltage, pressure gauge error and the standard deviation of repeat runs. The pore diameter errors have been reported separately in Fig. 4 and Fig. S2).

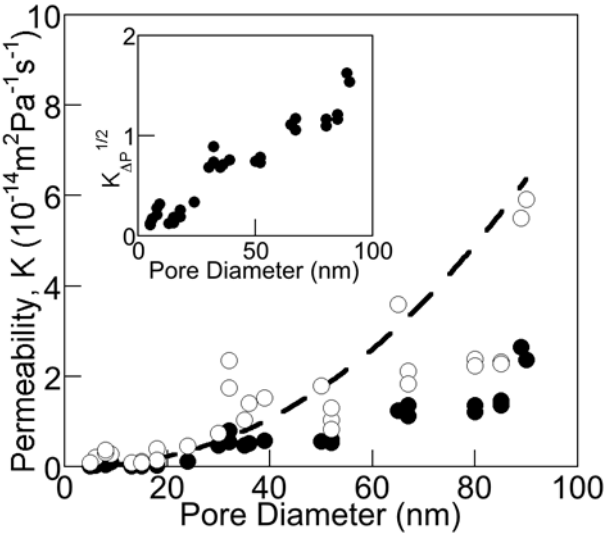

Fig. 3 Hydraulic permeability, K, as a function of membrane pore diameter for pressure-driven flow only ($K_{\Delta P}$, ●) and when V_{app} = 10 V was superimposed to the pressure driven flow (K_T , ○); electrolyte concentration and applied voltage are the same for all points; the dashed line is the theoretical K_T (Eq. 2). Inset: square root of $K_{\Delta P}$ variation with pore diameter.

When the EO-driven flow was imposed on the pressure-driven one a dramatic increase in the total flow rate for each pore diameter value was observed, especially for the smallest pores tested (~8 to 25 nm). While the pressure-driven flow decreases with the square of the pore size, EOF has no explicit dependence on D_p (Eq. 2). Therefore, the relative importance of the EOF over the total flow rate increases with decreasing pore size. This is more clearly observed when the ratio $K_{EO} / K_{\Delta P}$ as a

function of pore diameter is considered (Fig. 4). As the pore diameter decreases, membrane thickness and porosity also decrease, leading to an increase of the membrane resistance for the same applied voltage (Eq. 3). This translates in a reduced effective voltage and, hence, a lower electroosmotic pore velocity, u_{EO}. The electroosmotic mobility, though, is independent of the pore diameter (Fig. 4 inset), explaining the behaviour observed for $K_{EO} / K_{\Delta P}$ as a function of pore diameter. It should also be noted that for the same effective voltage, the EOF is independent of pore diameter (Fig. S4). The dashed black line in Fig. 4 represents EDL overlap ($2\lambda_D$ ~ 9 nm from Eq. 1). The same concentration (5 mM borate buffer) was used throughout the pore diameter study. Measurable EOF was clearly observed for all membranes, even with pore diameters at and below the EDL overlap region. Therefore, for membranes with progressively smaller pores, EO can be used to complement pressure-driven flow to increase overall liquid flow. EOF can be further increased, for the same applied voltage and pore diameter, by using a higher electrolyte concentration (Fig.S4).

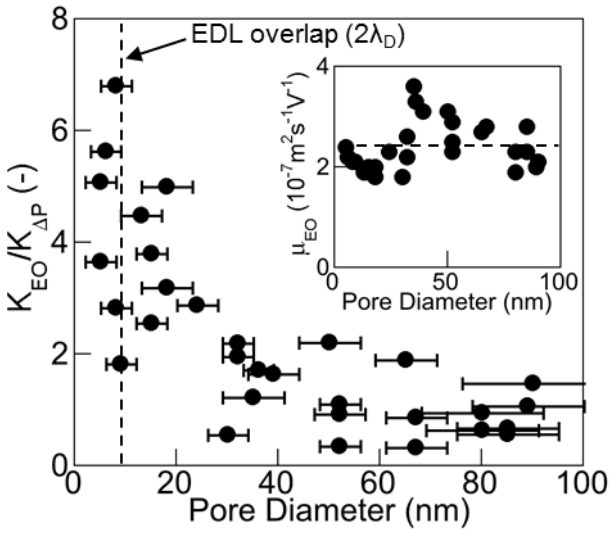

Fig. 4 Ratio of electroosmotic to pressure-driven permeability ($K_{EO} / K_{\Delta P}$) as a function of membrane pore diameter; the dashed vertical line indicates the Debye layer (EDL) overlap. Error in y-axis is 5% of each value. The inset shows the electroosmotic mobility, $m_{EO} = u_{EO} / E$, as a function of pore diameter.

As discussed in the introduction, no EOF is expected in pore diameters where there is EDL overlap. The asymmetric nature of the membranes with the smallest pore size could be the key to explain the results in Fig. 4. A recent experimental investigation on EOF-induced ion rectification in conical nanopores (similar in geometry to the asymmetric AAMs fabricated here) observed a larger than expected rectification factor for pores approaching the dimensions of the EDL (Yusko et al. 2010).

Moreover, a reduced or enhanced (depending on the direction of the electric field) ion permeability was predicted when an asymmetric distribution of ions was present along the pore (Cervera et al. 2007). Following this model, an increased conductance can be predicted for the negatively charged AAMs when the narrow opening of the membrane faces the anode. The net flow of cations (the counter-ions, Na^+) is directed to the larger pore diameter in the direction of flow away from the anode (which in this case it does) (Yusko et al. 2010). This supports the present results that an increase in pore conductance, due to the asymmetry of charge caused by the asymmetrical pore channel, enhanced the permeability of ions through the membrane, leading to the persistence of EOF in the EDL overlap region.

3.3 Concentration Polarisation and Regenerative EO pumping

Given the small pore size of the membranes used in this work (Fig. 2), significant concentration polarization is expected. This is confirmed by calculations of the Dukhin number, which is the ratio of surface to bulk conductivity (Zangle et al. 2009; Strickland et al. 2010), showing that it is greater than one for all membrane pore sizes examined (Fig. S5).

Concentration polarization with the same buffer solution used in this study has been observed in at the surface of microscale frits and electrodes (Suss et al. 2011; Strickland et al. 2010; Pu et al. 2004). Using a fluorescein solution local concentration changes were attributed to ion depletion zones within the system. The initial current behaviour, which induces a large increase in flow rate followed by a decrease over time (Fig. 5), observed here is also similar to the one observed in microchannels (Suss et al. (2011).

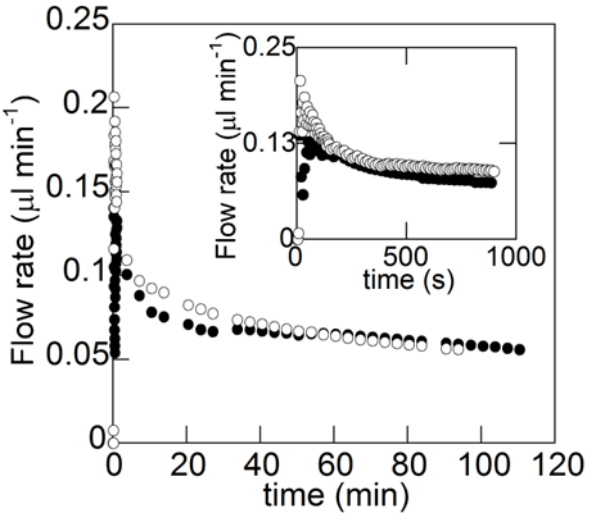

Fig. 5 Flow rate with time (●) a sharp initial increase and then a steady decrease in flow rate from a fresh run and (○) the repeated 2nd run, the flow rate with time is comparable to that of the 1st run indicating the EOF was regenerated. Inset: initial surge in flow rate zoomed in.

A simple model is proposed here to quantify the extent of concentration polarization over time. Experimental data shows that ΔV_{eff} is quasi-constant during the experiment. Eq. 3 therefore, is generalized as follows:

$$\Delta V_{eff} = \left(\Delta V_{app} - \Delta V_{dec}\right) - R_{tot} I \tag{5}$$

where $R_{tot} = R_{cp} + 2R_d$ is the total resistance of the EO process and R_{cp} is the resistance arising from concentration polarization. By substituting Eq. 4 in Eq. 2, the time dependence of R_{tot} can be obtained from experimental data (Fig. 6). The total resistance increases with time, with sudden current shocks leading to a decrease in R_{tot}, the resistance then restores until the next current shock, with a comparable slope. Current shocks were also observed in all experiments, accounting for some of the instabilities observed in flow (for example the slight deviations from steady state shown in Fig. 3 and Fig. 7). The presence of current shocks has been attributed to the propagation of concentration polarization, generating ion enrichment and depletion zones, away form the membrane surface (Suss et al. 2011; Mani et al. 2009). The sharp spikes in current were observed in the first and repeated runs for the regenerated EOF.

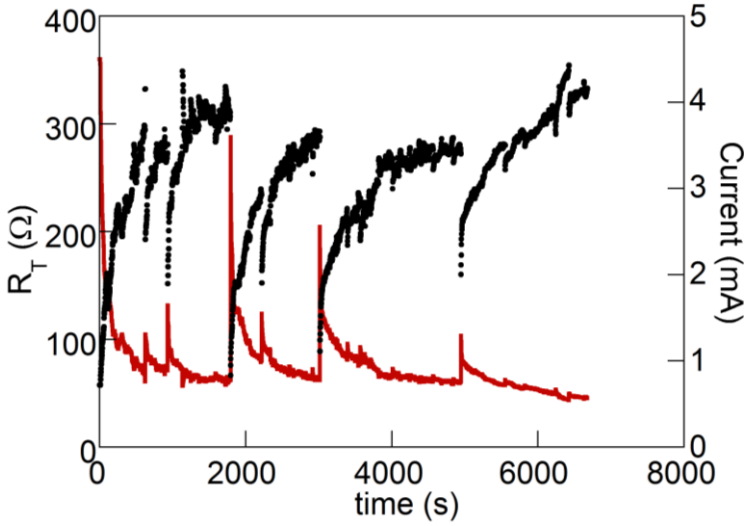

Fig. 6 Variation with time of total resistance (●) and current (—, red line) for 5mM $Na_2O_7B_4$, D_p = 67 nm and V_{app} = 10V Sudden decreases in total resistance are clearly linked to current shocks which disrupt the CP layer build-up, which is then resumed until the next current shock.

Although R_d cannot be measured directly, its value can be estimated by the value of R_{tot} at the beginning of the EO experiment, when significant CP has not yet developed. This yields R_d ~ 70 Ω.

As no weakening or thinning of the membrane was observed after more than 2 hours of operation (all membrane characterisation was completed post-EOF), R_d was assumed to be constant during the experimental time. The resistance given by the concentration polarization can then be calculated and, from this, the propagation of the CP enrichment layer can be estimated as $\delta_{cp} = \kappa A R_{cp}$, where δ_{cp} is the concentration polarization layer thickness, and κ the conductivity of the electrolyte. The membrane area coincides with the cross-section of the sample holder zone closest to the membrane. This section is approximately 1.6 cm long, ensuring that A can be considered constant. Although the electrical conductivity in the concentration polarization domain will vary due to local changes in the electrolyte concentration, the large reservoir volume (60 ml, Fig.1) will eventually compensate for any localized change. In the first approximation, therefore, the electrical conductivity can be considered constant, yielding a total thickness of the CP layer equal to 0.7 mm, with a propagation velocity of ~0.09 μm s^{-1}. These values are comparable to those obtained for a rectangular cross-sectional channel (Suss et al. 2011). An exact variation of the electrical conductivity as a function of local electrolyte concentration cannot be estimated using well-known models such as the Debye-Hückel or Onsager-Fuoss, due to the high concentration of the starting electrolyte (Wright 1988). Unfortunately no local measure of the electrolyte concentration near the membrane surface was possible.

Further proof that the reduction in flow was due to concentration polarisation was obtained when successful regeneration of EOF was achieved by physically turning the membrane holder and applying a pressure-driven flow, dislodging the ions which had built up on the surface of the membrane and redistributing them within the buffer solution. After this process the membrane holder was turned back to the original position to repeat the EO measurement. It can be clearly seen in Fig. 7 that with this procedure the EOF was able to recover to that of the original flow rate; however the EO pumps lifetime was reduced slightly. It is important to note here that the EO pump was able to pump liquid continuously without any change to experimental set-up (such as replenishing the buffer reservoir) for 2 hours (and 4 hours including the regeneration experiment), which is a considerable improvement in EO pump lifetimes compared with previous studies (Brask et al. 2005; Kwon et al. 2012). Similar results to these have been obtained for membranes of pore diameters down to ~ 10 nm. The regeneration therefore confirms that the reduction in flow rate was caused by concentration polarisation at the membrane surface and that this can be overcome by sweeping the accumulated ion layer away from the membrane surface, thereby replenishing the depleted zones with buffer solution.

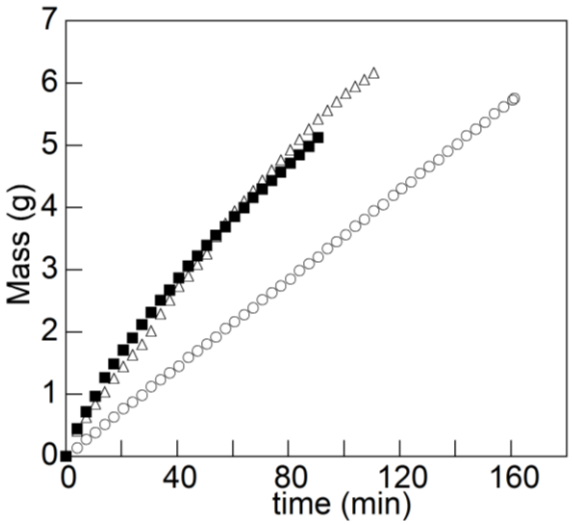

Fig. 7 Mass versus time plots for an AAM recovering flow rates after concentration polarisation for a 67 nm average pore diameter AAM, (○) when no voltage is applied, (Δ) when V_{app} = 10 V is superimposed onto the pressure-driven flow for the first run and (■) when V_{app} = 10 V after the build-up of ions has been flushed from the surface of the membrane.

4. Conclusions

Nanoporous AAMs were prepared via electrochemical aluminium anodization where the pore diameter of the membrane was accurately controlled, enabling a systematic investigation of EO at the nanoscale. The AAMs had narrow pore distributions and the pore diameter of the membranes ranged from ~8 to 100 nm. Enhanced flow was observed for the electroosmotic flow rates when compared to pressure-driven flow rates alone, and this was most significant (up to 5 times) for the smallest pore diameters (~8 to 25 nm) tested, where the pore diameter was approaching EDL overlap. For the smallest pore diameters produced (~8 nm) EO was still observed even with EDL overlap. Achieving stable electroosmotic flows at lower ionic concentrations proved challenging due to concentration polarisation and ion depletion in the buffer; however a stable EOF for up to 2 hours was achieved for several membranes of different pore diameters. The electroosmotic flow was found to increase with increasing buffer concentration. A significant difference between the applied and effective voltage was responsible for low thermodynamic efficiency observed, up to 1.0 %, in line with previous findings.

Nonetheless, for the smallest pore diameters tested, EO pumping could be used as a support for mechanical pumping even for larger scale applications as well as current lab-on-a-chip systems.

Acknowledgements

The authors acknowledge the UK EPSRC EP/6045798/1 grant for funding. DM is supported by a UK Royal Academy of Engineering Research Fellowship. The authors acknowledge John Bishop for his electronics expertise and support and the Microscopy and Analysis Suite at the University of Bath.

References

Besteman K, Zevenbergen MAG, Heering HA, Lemay SG (2004) Direct Observation of Charge Inversion by Multivalent Ions as a Universal Electrostatic Phenomenon. Phys Rev Lett 93 (17):170802

Brask A, Kutter JP, Bruus H (2005) Long-term stable electroosmotic pump with ion exchange membranes. Lab Chip 5 (7):730-738

Bruus H (2007) Theoretical Microfluidics (Oxford Master Series in Physics). Oxford University Press, USA.

Cao Z, Yuan L, Liu YF, Yao S, Yobas L (2012) Microchannel plate electro-osmotic pump. Microfluid Nanofluid 13 (2):279-288

Cervera J, Alcaraz A, Schiedt B, Neumann R, Ramírez P (2007) Asymmetric Selectivity of Synthetic Conical Nanopores Probed by Reversal Potential Measurements. J Phys Chem C 111 (33):12265-12273

Chang H-C, Yeo LY (2010) Electrokinetically-Driven Microfluidics and Nanofluidics. Cambridge University Press, United States of America

Chen Y-F, Hu Y-H, Chou Y-I, Lai S-M, Wang C-C (2010) Surface modification of nano-porous anodic alumina membranes and its use in electroosmotic flow. Sensor Actuat B Chem 145 (1):575-582

Chen Y-F, Li M-C, Hu Y-H, Chang W-J, Wang C-C (2008a) Low-voltage electroosmotic pumping using porous anodic alumina membranes. Microfluid Nanofluid 5 (2):235-244

Chen Y, Ni Z, Wang G, Xu D, Li DY (2008b) Electroosmotic Flow in Nanotubes with High Surface Charge Densities. Nano Lett 8 (1):42-48

Chuan-Hua C, Santiago JG (2002) A planar electroosmotic micropump. J Microelectromech S 11 (6):672-683

Corti H, Crovetto R, Fernandez-Prini R (1980) Properties of the borate ion in dilute aqueous solutions. J Chem Soc Farad T 1 76 (0):2179-2186

Erlandsson PG, Robinson ND (2011) Electrolysis-reducing electrodes for electrokinetic devices. Electrophoresis 32 (6-7):784-790

Freund JB (2002) Electro-osmosis in a nanometer-scale channel studied by atomistic simulation. J Chem Phys 116 (5):2194-2200

Hernandez A, Martinez F, Martín A, Prádanos P (1995) Porous Structure and Surface Charge Density on the Walls of Microporous Alumina Membranes. J Colloid Interf Sci 173 (2):284-296

Huang K-D, Yang R-J (2007) Electrokinetic behaviour of overlapped electric double layers in nanofluidic channels. Nanotechnology 18 (11):115701

Hunter RJ (1981) Zeta potential in colloid science. Academic Press, London

Kemery PJ, Steehler JK, Bohn PW, (1998) Electric field mediated transport in nanometer diameter channels. Langmuir 14 (10):2884-2889

Kwon K, Park C-W, Kim D (2012) High-flow rate, compact electroosmotic pumps with porous polymer track-etch membranes. Sensors Actuat A Phys 175 (0):108-115

Lee KP, Leese H, Mattia D (2012) Water flow enhancement in hydrophilic nanochannels. Nanoscale 4 (8):2621-2627

Lee KP, Mattia D (2013) Monolithic nanoporous alumina membranes for ultrafiltration applications: Characterization, selectivity-permeability analysis and fouling studies. J Membrane Sci http://dx.doi.org/10.1016/j.memsci.2013.01.051

Lillo M, Losic D (2009) Pore opening detection for controlled dissolution of barrier oxide layer and fabrication of nanoporous alumina with through-hole morphology. J Membrane Sci 327 (1-2):11-17

Mani A, Zangle TA, Santiago JG (2009) On the Propagation of Concentration Polarization from Microchannel−Nanochannel Interfaces Part I: Analytical Model and Characteristic Analysis. Langmuir 25 (6):3898-3908

Masuda H, Fukuda K (1995) Ordered Metal Nanohole Arrays Made by a Two-Step Replication of Honeycomb Structures of Anodic Alumina. Science 268 (5216):1466-1468

Nielsch K, Choi J, Schwirn K, Wehrspohn RB, Gosele U (2002) Self-ordering Regimes of Porous Alumina: The 10 Porosity Rule. Nano Lett 2 (7):677-680

Prakash P, Grissom MD, Rahn CD, Zydney AL (2006) Development of an electroosmotic pump for high performance actuation. J Membrane Sci 286 (1-2):153-160

Pu Q, Yun J, Temkin H, Liu S (2004) Ion-Enrichment and Ion-Depletion Effect of Nanochannel Structures. Nano Lett 4 (6):1099-1103

Rice CL, Whitehead R (1965) Electrokinetic Flow in a Narrow Cylindrical Capillary. J Phys Chem 69 (11):4017-4024

Romero V, Vega V, García J, Prida VM, Hernando B, Benavente J (2012) Ionic transport across tailored nanoporous anodic alumina membranes. J Colloid Interf Sci 376 (1):40-46

Strickland DG, Suss ME, Zangle TA, Santiago JG (2010) Evidence shows concentration polarization and its propagation can be key factors determining electroosmotic pump performance. Sensor Actuat B Chem 143 (2):795-798

Sulka GD (2008) Highly Ordered Anodic Porous Alumina Formation by Self-Organized Anodizing. In: Eftekhari A (ed) Nanostructured Materials in Electrochemistry, 1st edn. Wiley-VCH Verlag GmbH & Co KGaA, Weinheim, Germany, pp 1-116

Suss ME, Mani A, Zangle TA, Santiago JG (2011) Electroosmotic pump performance is affected by concentration polarizations of both electrodes and pump. Sensor Actuat A Phys 165 (2):310-315

Takamura Y, Onoda H, Inokuchi H, Adachi S, Oki A, Horiike Y (2003) Low-voltage electroosmosis pump for stand-alone microfluidics devices. Electrophoresis 24 (1-2):185-192

Tang F, Fudouzi H, Uchikoshi T, Sakka Y (2004) Preparation of porous materials with controlled pore size and porosity. J Eur Ceram Soc 24 (2):341-344

Vajandar SK, Xu D, Markov DA, Wikswo JP, Hofmeister W, Li D (2007) SiO_2 coated porous anodic alumina membranes for high flow rate electroosmotic pumping. Nanotechnology 18 (27):275705

Wright MR (1988) The Nature of Electrolyte Solutions. Dimensions of Science. Macmillan Education Ltd.

Wu J, Gerstandt K, Majumder M, Zhan X, Hinds BJ (2011) Highly efficient electroosmotic flow through functionalized carbon nanotube membranes. Nanoscale 3 (8):3321-3328

Yao S, Hertzog DE, Zeng S, Mikkelsen Jr JC, Santiago JG (2003) Porous glass electroosmotic pumps: design and experiments. J Colloid Interf Sci 268 (1):143-153

Yao S, Myers AM, Posner JD, Rose KA, Santiago JG (2006) Electroosmotic pumps fabricated from porous silicon membranes. J Microelectromech S 15 (3):717-728

Yusko EC, An R, Mayer M (2010) Electroosmotic Flow Can Generate Ion Current Rectification in Nano- and Micropores. ACS Nano 4 (1):477-487

Zangle TA, Mani A, Santiago JG (2009) On the Propagation of Concentration Polarization from Microchannel−Nanochannel Interfaces Part II: Numerical and Experimental Study. Langmuir 25 (6):3909-3916

Zeng S, Chen C-H, Mikkelsen Jr JC, Santiago JG (2001) Fabrication and characterization of electroosmotic micropumps. Sensor Actuat B Chem 79 (2–3):107-114